Supporting Information for

Designing a family of 2D kagome monolayer $B_{18}S_8$, $B_{18}S_8H_2$, $B_{18}S_6X_2$ (X=Cl, Br, I) with tunable Dirac cones and high Fermi velocity

Su-Yang Shen,[1] En-Qi Bao,[1] Xing-Yu Wang,[1,2] Jiafu Wang,[1,2,*] and Jun-Hui Yuan,[1,*]

[1]School of Physics and Mechanics, Wuhan University of Technology, Wuhan 430070, China

[2]School of Materials and Microelectronics, Wuhan University of Technology, Wuhan 430070, China

[*]**Corresponding Author**

E-mail: jasper@whut.edu.cn (J. Wang); yuanjh90@163.com (J.-H. Yuan)

Note 1. Details for computational method.

The calculations employed the projector augmented-wave (PAW) method[1,2], seamlessly integrated within the VASP code[3,4]. The valence electron configurations were specified as follows: 1s for H, 2s and 2p for B, 3s and 3p for S, 3s and 3p for Cl, 4s and 4p for Br, 5s and 5p for I. A plane wave cutoff energy of 500 eV was established for these configurations. For the determination of the exchange-correlation energy, the generalized gradient approximation (GGA) within the Perdew-Burke-Ernzerhof (PBE) scheme was adopted[5]. During the structural optimization phase, stringent criteria were imposed, including a force criterion of 0.001 eV/Å in any direction, an energy criterion of 10^{-7} eV, and the utilization of a dense 11×11×1 Γ-centered *k*-mesh. Furthermore, to avoid the interactions between adjacent layers,[6–8] the a vacuum slab of up to 20 Å was introduced for all 2D structures along the z-direction. Additionally, phonon dispersion, grounded in density functional perturbation theory (DFPT), was computed using *Phonopy*[9] software. The VASPKIT code[10] served as a valuable tool in facilitating the data analysis process.

Note 2. Calculated method for Young's modulus *Y* and Poisson's ratio *v*.

For the angle dependent in-plane Young's modulus (Y) and Poisson's ratio (υ) are calculated using the independent elastic constants (C_{11}, C_{22}, C_{12} and C_{66}). The calculation formula is as follows:[11]

$$Y(\theta) = \frac{C_{11}C_{22} - C_{12}^2}{C_{11}sin^4\theta + C_{22}cos^4\theta + \left(\frac{C_{11}C_{22} - C_{12}^2}{C_{66}} - 2C_{12}\right)cos^2\theta sin^2\theta}$$

$$\nu(\theta) = \frac{C_{12}(sin^4\theta + cos^4\theta) - (C_{11} + C_{22} - \frac{C_{11}C_{22} - C_{12}^2}{C_{66}})cos^2\theta sin^2\theta}{C_{11}sin^4\theta + C_{22}cos^4\theta + \left(\frac{C_{11}C_{22} - C_{12}^2}{C_{66}} - 2C_{12}\right)cos^2\theta sin^2\theta}$$

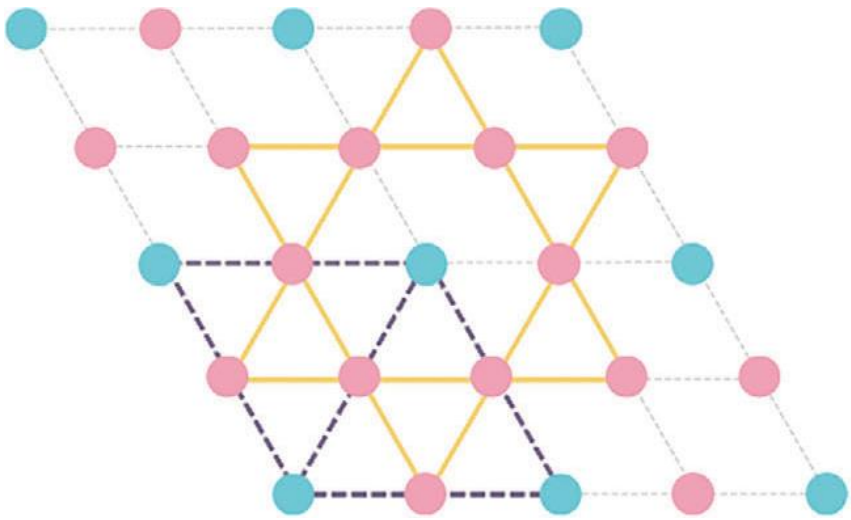

Fig. S1. Schematic diagram of constructing a kagome lattice from a triangular lattice based on the "1+3" strategy.

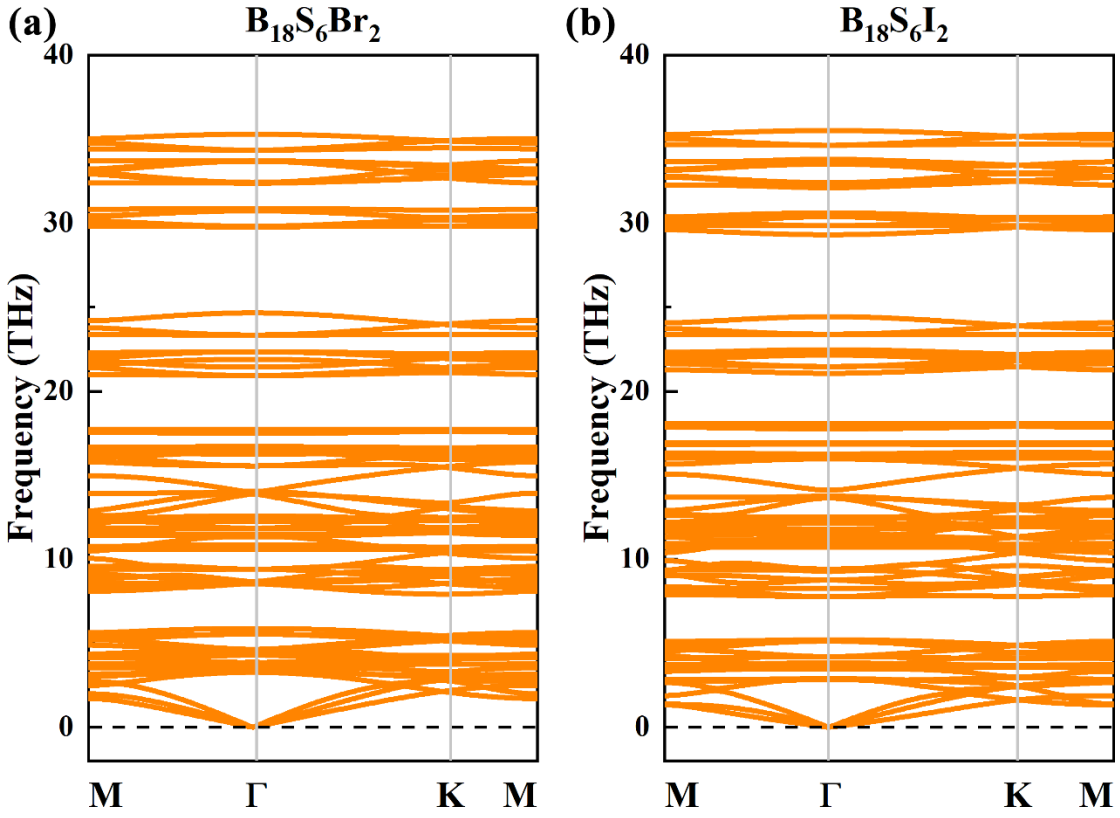

Fig. S2. Phonon dispersions of states of (a) $B_{18}S_6Br_2$ and (b) $B_{18}S_6I_2$ monolayers.

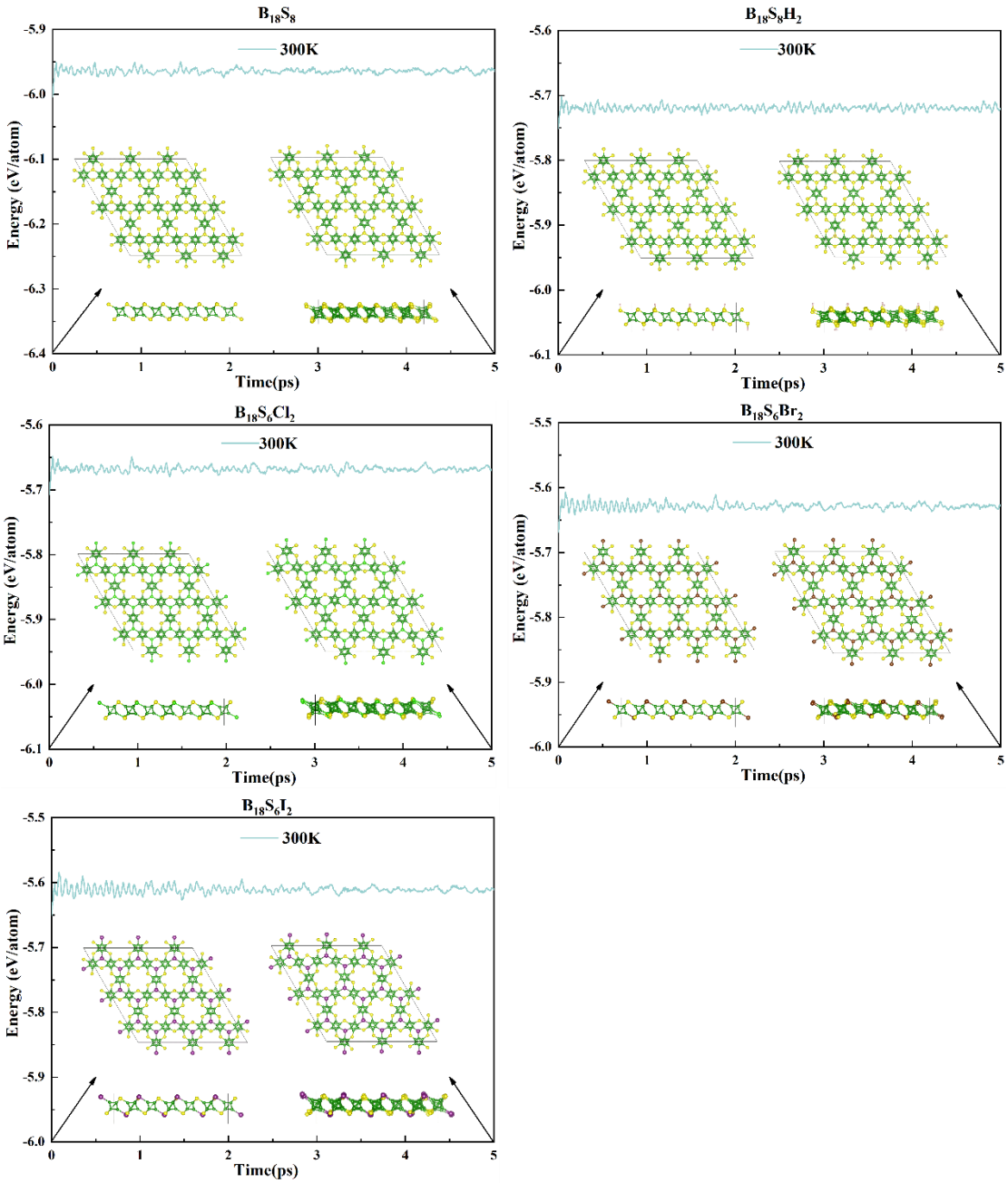

Fig. S3. AIMD simulations of $B_{18}S_8$, $B_{18}S_8H_2$, $B_{18}S_6X_2$ (X = Cl, Br, I) monolayers at 300 K.

Table S1. Calculated independent elastic constants C_{ij} of $B_{18}S_8$, $B_{18}S_8H_2$, $B_{18}S_6X_2$ (X = Cl, Br, I) monolayers.

Materials	C_{11}/C_{22}	C_{12}	C_{66}	$C_{11}C_{22} - C_{12}^2 > 0$
$B_{18}S_6$	118.46	28.45	45.01	True
$B_{18}S_8$	66.52	20.30	23.11	True
$B_{18}S_8H_2$	72.76/72.81	25.12	23.83	True
$B_{18}S_6Cl_2$	59.40	16.62	21.39	True
$B_{18}S_6Br_2$	54.57	15.34	19.62	True
$B_{18}S_6I_2$	51.92	14.54	18.71	True

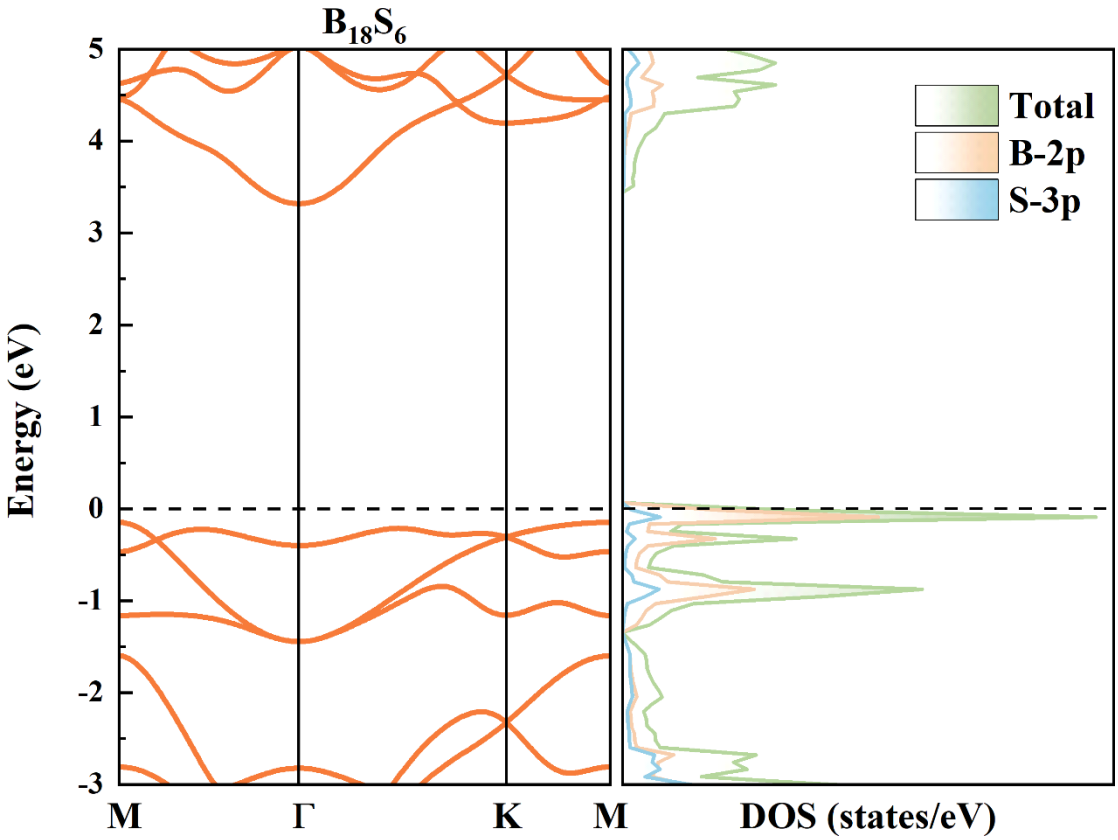

Fig. S4. Band structure and density of states of $B_{18}S_6$ monolayer using the primitive cell based on GGA-PBE calculations.

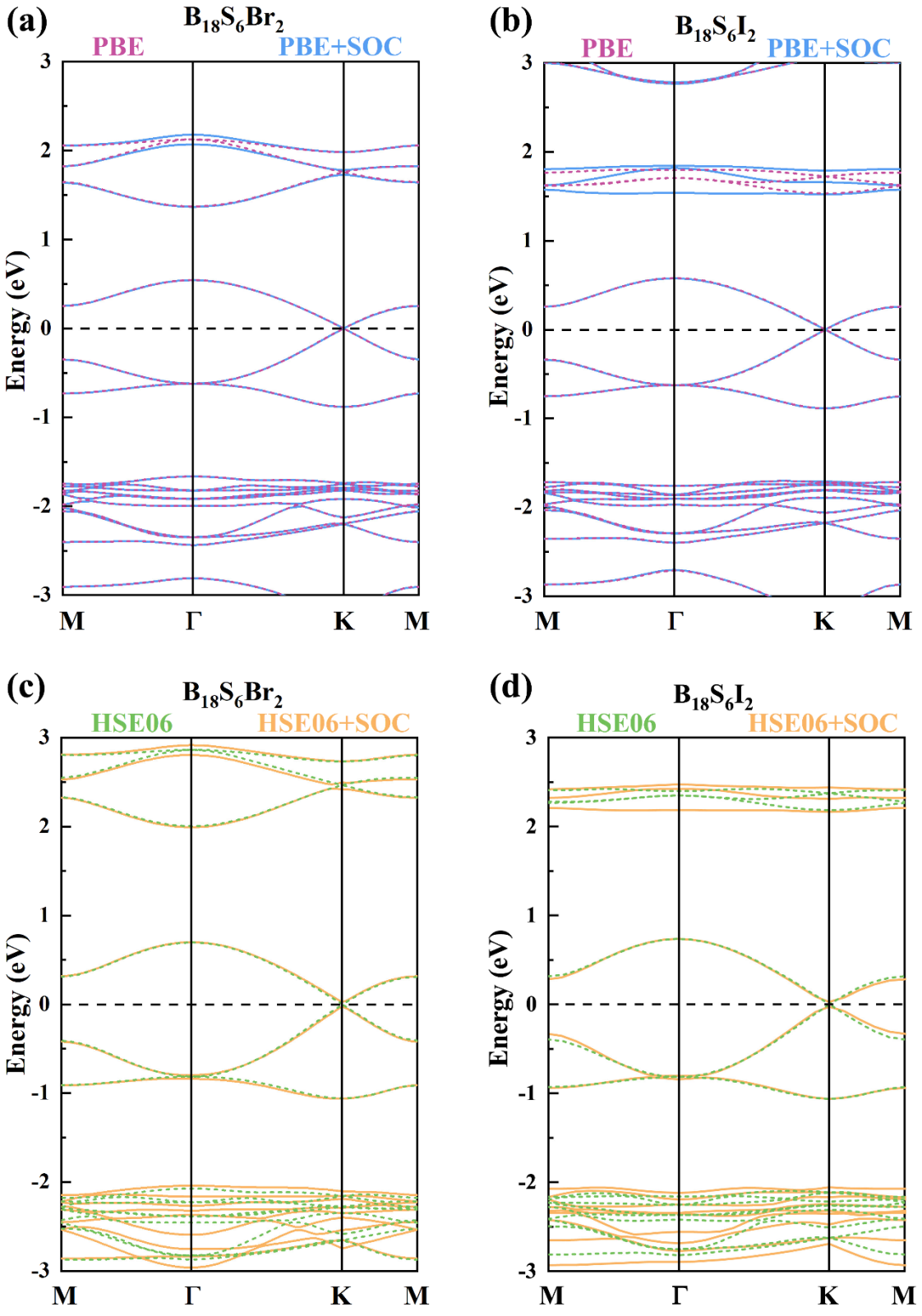

Fig. S5. Band structure of $B_{18}S_6Br_2$ and $B_{18}S_6I_2$ monolayer based on GGA-PBE and HSE06 calculations with/without SOC effect considered.

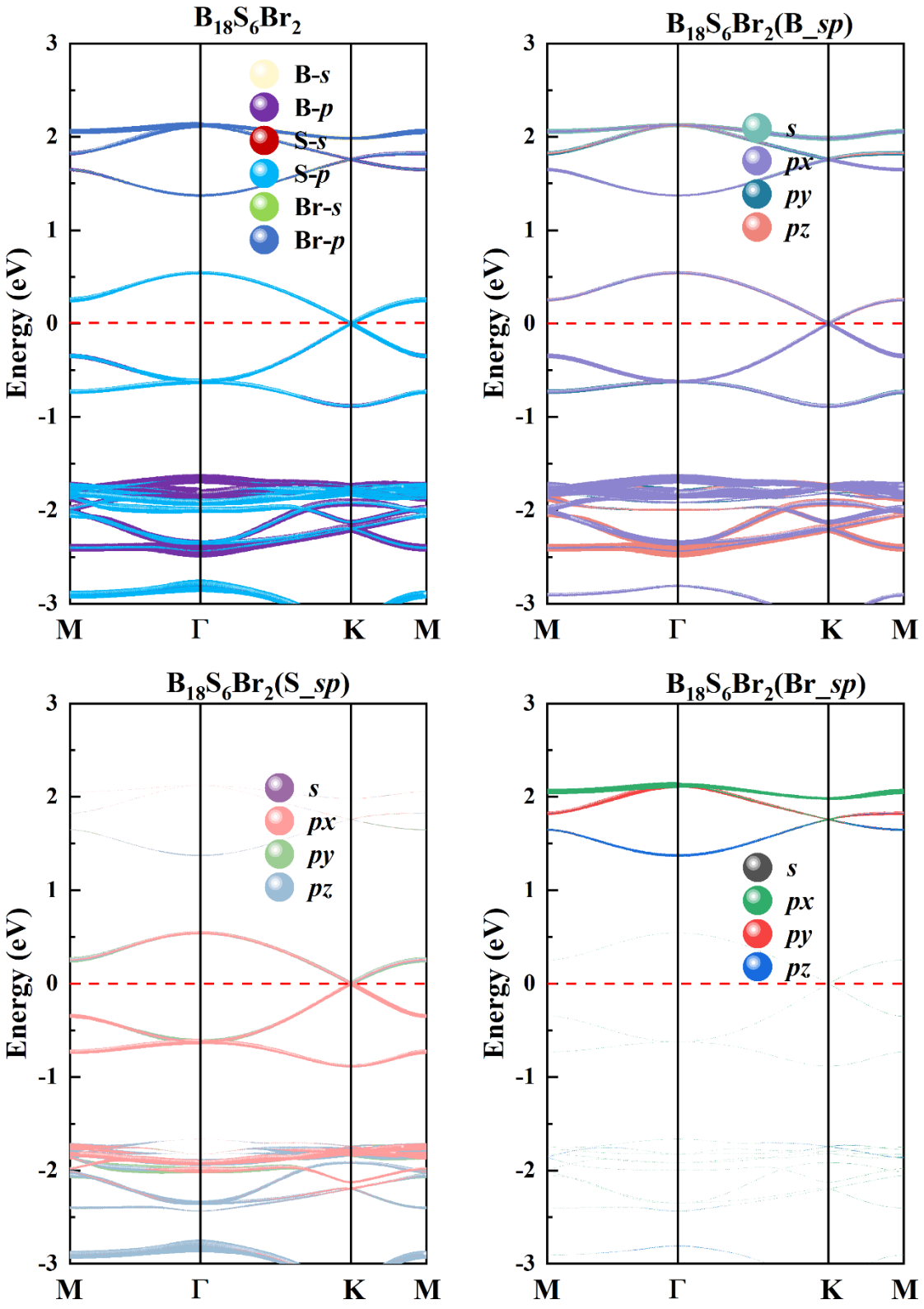

Fig. S6. Projected band structures of $B_{18}S_6Br_2$ monolayer based on GGA-PBE calculations.

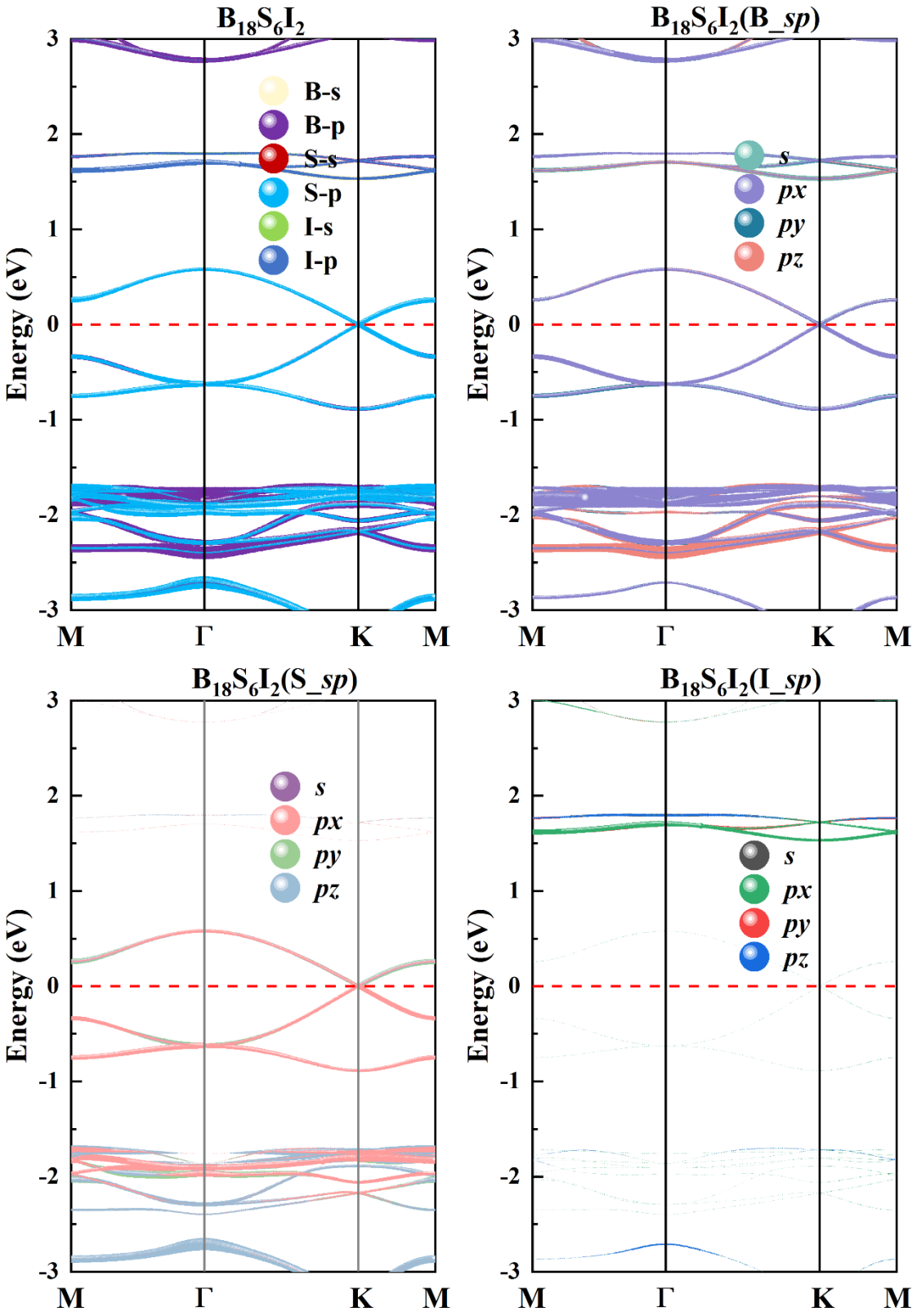

Fig. S7. Projected band structures of $B_{18}S_6I_2$ monolayer based on GGA-PBE calculations.

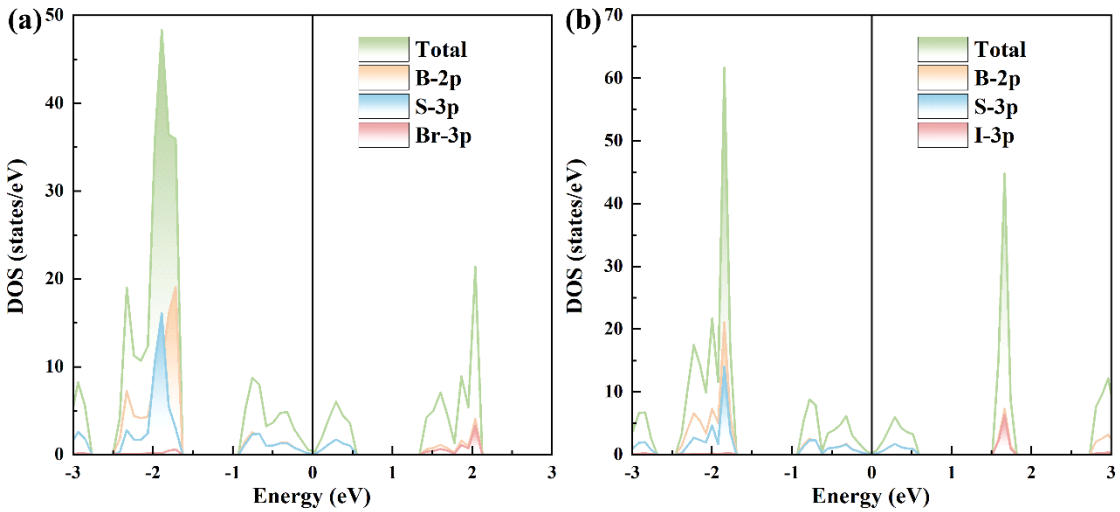

Fig. S8. Density of states of (a) $B_{18}S_6Br_2$ and $B_{18}S_6I_2$ monolayers based on GGA-PBE calculations.

Table S2. Calculated Fermi velocity at the Dirac cone of $B_{18}S_8$, $B_{18}S_8H_2$ and $B_{18}S_6X_2$ (X= Cl, Br, I) monolayers along Γ-K and K-M direction.

Materials	V_F^{G-K}	V_F^{K-M}
$B_{18}S_8$	2.716×10^5 m/s	2.690×10^5 m/s
$B_{18}S_8H_2$	2.947×10^5 m/s	2.930×10^5 m/s
$B_{18}S_6Cl_2$	2.873×10^5 m/s	2.840×10^5 m/s
$B_{18}S_6Br_2$	2.961×10^5 m/s	2.941×10^5 m/s
$B_{18}S_6I_2$	3.067×10^5 m/s	3.046×10^5 m/s

Table S3. Calculated Fermi velocities for some 2D Dirac semimetals.

Materials	V_F (10^5 m/s)	References
graphene	8.22	[12]
g-SiC_6	7.11	[13]
g-SiC_3	6.0	[14]
$ClPC_6$	6.31	[15]
$ClPC_3$	5.11	[16]
HPC_6	7.5	[17]

References

[1] P.E. Blöchl, Projector augmented-wave method, Phys. Rev. B 50 (1994) 17953–17979. https://doi.org/10.1103/PhysRevB.50.17953.

[2] G. Kresse, D. Joubert, From ultrasoft pseudopotentials to the projector augmented-wave method, Phys. Rev. B 59 (1999) 1758–1775. https://doi.org/10.1103/PhysRevB.59.1758.

[3] G. Kresse, J. Furthmüller, Efficiency of ab-initio total energy calculations for metals and semiconductors using a plane-wave basis set, Computational Materials Science 6 (1996) 15–50. https://doi.org/10.1016/0927-0256(96)00008-0.

[4] G. Kresse, J. Furthmüller, Efficient iterative schemes for *ab initio* total-energy calculations using a plane-wave basis set, Phys. Rev. B 54 (1996) 11169–11186. https://doi.org/10.1103/PhysRevB.54.11169.

[5] J.P. Perdew, K. Burke, M. Ernzerhof, Generalized Gradient Approximation Made Simple, Phys. Rev. Lett. 77 (1996) 3865–3868. https://doi.org/10.1103/PhysRevLett.77.3865.

[6] Y.-Q. Song, J.-H. Yuan, L.-H. Li, M. Xu, J.-F. Wang, K.-H. Xue, X.-S. Miao, KTlO: a metal shrouded 2D semiconductor with high carrier mobility and tunable magnetism, Nanoscale 11 (2019) 1131–1139. https://doi.org/10.1039/C8NR08046A.

[7] H. Lang, S. Zhang, Z. Liu, Mobility anisotropy of two-dimensional semiconductors, Phys. Rev. B 94 (2016) 235306.

https://doi.org/10.1103/PhysRevB.94.235306.
[8] Y.-Q. Song, J.-H. Yuan, L.-H. Li, M. Xu, J.-F. Wang, K.-H. Xue, X.-S. Miao, KTlO: a metal shrouded 2D semiconductor with high carrier mobility and tunable magnetism, Nanoscale 11 (2019) 1131–1139. https://doi.org/10.1039/C8NR08046A.
[9] A. Togo, I. Tanaka, First principles phonon calculations in materials science, Scripta Materialia 108 (2015) 1–5. https://doi.org/10.1016/j.scriptamat.2015.07.021.
[10] V. Wang, N. Xu, J.-C. Liu, G. Tang, W.-T. Geng, VASPKIT: A user-friendly interface facilitating high-throughput computing and analysis using VASP code, Computer Physics Communications 267 (2021) 108033. https://doi.org/10.1016/j.cpc.2021.108033.
[11] J.-H. Yuan, K.-H. Xue, J.-F. Wang, X.-S. Miao, Gallium Thiophosphate: An Emerging Bidirectional Auxetic Two-Dimensional Crystal with Wide Direct Band Gap, J. Phys. Chem. Lett. 10 (2019) 4455–4462. https://doi.org/10.1021/acs.jpclett.9b01611.
[12] L.-C. Xu, R.-Z. Wang, M.-S. Miao, X.-L. Wei, Y.-P. Chen, H. Yan, W.-M. Lau, L.-M. Liu, Y.-M. Ma, Two dimensional Dirac carbon allotropes from graphene, Nanoscale 6 (2014) 1113–1118. https://doi.org/10.1039/C3NR04463G.
[13] T. Yang, X. Jiang, W. Yi, X. Cheng, X. Liu, A g-SiC 6 monolayer and its analogs: A new class of tunable Dirac cone materials and novel quantum spin Hall insulators, Applied Surface Science 578 (2022) 151986. https://doi.org/10.1016/j.apsusc.2021.151986.
[14] X. Qin, Y. Wu, Y. Liu, B. Chi, X. Li, Y. Wang, X. Zhao, Origins of Dirac cone formation in AB3 and A3B (A, B = C, Si, and Ge) binary monolayers, Sci Rep 7 (2017) 10546. https://doi.org/10.1038/s41598-017-10670-x.
[15] W. Yi, X. Jiang, Z. Wang, T. Yang, B. Yang, X. Liu, ABX6 Monolayers: A new Dirac material family containing high Fermi velocities and topological properties, Applied Surface Science 570 (2021) 151237. https://doi.org/10.1016/j.apsusc.2021.151237.
[16] X. Jiang, T. Yang, G. Fei, W. Yi, X. Liu, Novel Two-Dimensional ABX_3 Dirac Materials: Achieving a High-Speed Strain Sensor via a Self-Doping Effect, J. Phys. Chem. Lett. 13 (2022) 676–685. https://doi.org/10.1021/acs.jpclett.1c03829.
[17] H.-Y. Lu, N. Jiao, B.-W. Li, W.-C. Yi, P. Zhang, Hydrogenated group IV-V monolayer HAB6: A new type of Dirac material constructed by isoelectronic rule, Applied Surface Science 554 (2021) 149635. https://doi.org/10.1016/j.apsusc.2021.149635.